Engineering Plasmonic Nanostructures for label-free SERS Detection of Neurotoxic Gases

[1,2] K. Batista, [1,2] M. Lafuente, [1,3] S.G. Rodrigo [1,2,4] R. Mallada, [1,2,4] M.P. Pina

[1]Instituto de Nanociencia y Materiales de Aragón (INMA), CSIC-Universidad de Zaragoza, 50009 Zaragoza, Spain

[2] Department of Chemical & Environmental Engineering, University of Zaragoza, 50018 Zaragoza, Spain

[3] Department of Applied Physics, Sciences Faculty, University of Zaragoza, 50009 Zaragoza, Spain

[4] Networking Research Center on Bioengineering, Biomaterials and Nanomedicine, CIBER-BBN, 28029 Madrid, Spain.

E-mail address of the corresponding author: mapina@unizar.es

ORCID number of the corresponding author: 0000-0001-9897-6527

***Abstract*—In this work, we explore the SERS based sensing capabilities of core-shell nanostructures for gas detection of neurotoxic agents at ppm level. These nanostructures generate intense localized surface plasmon resonances which are engineered by tuning geometrical parameters, in particular the aspect ratio of the metallic nanorods and the thickness of the silica mesoporous shell to extend the spectral window for the SERS based sensing from the visible to the near-infrared. This nanoarchitecture enables the integration of sampling preconcentration and detection of Sarin gas surrogate in a single SERS unit.**

Keywords—Surface Enhanced Raman Spectroscopy, Gas sensing, core-shell nanoparticles, metallic nanorods, LSPR tuning, preconcentration

I. Introduction

The detection of neurotoxic agents in the environment is of extreme importance for defence and homeland security nowadays [1]. Some of these agents, for instance, sarin, presents an immediately dangerous to life or health (IDLH) of 0.2 mg/m^3 (0.03 ppm) which exposure can lead to seizure and death [2]. For achieving such low detection limits, the combination of cumbersome analytical techniques, such as GC-MS and SPME [3], IMS and SPME [4], IMS and ESI [4], IMS and PCSI [5] are commonly necessary. First responders (FRs) still need technologically advanced tools and equipment that are affordable, lightweigh and easy to use for rapid detection, identification, and monitoring (DIM) of hazardous agents on the scene to facilitate timely and appropriate actions in the event of a chemical incident. A promising cost-effective technique that allows for non-destructive, selective, ultrasensitive, and multiplexed detection is the Surface-Enhanced Raman Spectroscopy (SERS) [6]. Previous works reported the Raman spectra of chemical warfare agents (CWAs) in liquid or solid state using a portable Raman spectrometer [7].

Overall, the application of SERS for gas phase detection is severely constrained by the occurrence of hot spots in very close vicinity (< 10 nm) to the plasmonic surface. Interestingly, more recent studies have been conducted regarding the detection in gas state with Raman/SERS, achieving satisfactory detection limits of 2.5-0.13 ppmV for Sarin gas surrogate [6], [8], [9]. When molecules do not show any affinity for the plasmonic surface, the most common strategy for label-free SERS detection is molecular trapping by physical or chemical adsorption. To this purpose, nanoporous materials may be used to concentrate gaseous molecules close to the surface, increasing the sensitivity of the SERS sensor. Thus, the combination of (semi-conductor) micro-mesoporous structures such as TiO_2, SiO_2 and ZnO, with metallic Au/Ag nanoparticles in a core-shell or film structure is becoming a quite popular strategy [10], [11], [12], [13]. These core-shell systems have been already demonstrated in the literature for SERS detection of the chemical dimethyl methylphosphonate (DMMP), a G-series nerve agent simulant with lower toxicity [12]–[14].

In this work, the core-shell system having the Au@Ag nanorods as the cores and a mesoporous silica layer on the shell, denoted as Au@Ag@mSiO_2, is explored for the SERS based sensing of neurotoxic agents. More specifically, the size, aspect ratio and spatial arrangement of Au@Ag@mSiO_2 nanoparticles are fully investigated pursuing higher enhancement factors and the fine tuning of their LSPRs for the fabrication of portable SERS based sensors.

II. Materials and Methods

A. Preparation of SERS substrates based on Au@Ag@mSiO_2

The preparation of Au@Ag@mSiO_2 can be described in six main steps, as seen in Figure II-1. The Au nanorod is synthesized following a seed mediation method described elsewhere [17], with minor modifications. For the Au@Ag configuration, a silver shell must be grown on the Au nanorods. This step is monitored by UV-VIS. The reaction time is controlled by the LSPR band position and is stopped at a desired wavelength.

The synthesis of the mesoporous shell is performed on freshly-synthesized Au@Ag nanorods. First, a CTAB solution is prepared in warm condition. After complete dissolution, the addition of absolute ethanol is followed, maintaining the agitation. After the stabilization of CTAB in ethanol, NH_3 is then incremented followed by the Au@Ag batch, added dropwise and at a higher agitation speed. Under a very high agitation speed, the silica precursor tetraethyl orthosilicate (TEOS) is finally integrated, in dropwise mode, with a molar ratio of Au/TEOS 9.3. The template (CTAB) removal can be

2022 IEEE Sensors | 978-1-6654-8464-0/22/$31.00 ©2022 IEEE | DOI: 10.1109/SENSORS52175.2022.9967361

performed by two different cation exchange methods. The first one, referred as reflux, is a temperature mediated reflux at 78 ºC with ethanolic solution of NH_4NO_3 (35 mM), maintained for 24h. The second one [19], referred as ultrasonication, is by ultrasonication cycles: two using NH_4NO_3 solution (75 mM), and three with ethanol for washing. In both methods, nanoparticles are resuspended in ethanol and stored at ambient temperature in the dark.

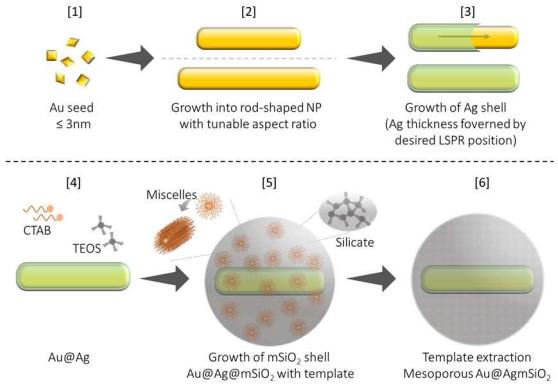

Figure II-1. Scheme of the Au and Au@Ag nanorods synthesis and Au@Ag@mSiO₂ mesoporous system.

Finally, the Au@Ag@mSiO$_2$ nanoparticles are deposited, by spin-coating method, on clean transparent cover-glass (⌀15 mm, 1 mm thick). An adhesive shadow mask (⌀15 mm with ⌀ 8mm hole mid centered) is used for reducing the deposition area. Previous the spin-coating cycles, substrates are pre-heated for a short time. After every spin coating, the substrate is heated again for nanoparticle film annealing. This cycle is repeated as many times as desired.

The SERS performance of the as-prepared SERS substrates was evaluated by the analytical enhancement factor (AEF) using the standard Raman active molecule, 4-nitrobenzenothiol (or 4-thiophenol, 4-NBT) as described in our previous works [6], [8]. Shortly, the AEF can be defined as:

$$AEF = (I_{SERS} \times C_{Raman}) / (I_{Raman} \times C_{SERS}) \qquad (1)$$

Where C_{Raman} and C_{SERS} are the 4-NBT concentrations in the Raman (10 mM) and SERS conditions (1 µM) respectvely. And I_{Raman} and I_{SERS} (cts.cm^2/kW.s) are the intensity of 4-NBT peak at approximately 1332 cm^{-1} (NO_2 stretching mode) from the 10 mM solution and from the Au@MCM48 SERS substrates with 4-NBT at 1 µM respectively.

B. SERS detection in Gas Phase of Sarin Surrogate

The SERS measurements were conducted in a microfluidic gas chamber (2.7×10^{-2} cm^3), where a N_2 gas stream of 10 mL/min with 2.5 ppmV (14 mg/m^3) of DMMP was fed continuously [6], [8]. DMMP has a strong peak at approximately 715 cm^{-1} related to symmetrical (P–CH_3) stretching mode and will be the one used as a reference in this work. Both Raman and SERS experiments were performed using the Alpha 300 Raman spectrometer (WITec) with a confocal optical microscope. All spectra were recorded at room temperature with 785 nm laser line and x10 lens. Raman measurements used laser power of 50 mW and 10 s. of acquisition time, while SERS measurements used 0.35 mW and 0.1s. acquisition time. SERS measurements were performed as a mapping, with area of 200 x 200 µm^2 and 100 acquisition points per area.

III. EXPERIMENTAL RESULTS

The standard Au nanorods synthesis (Figure III-1A) resulted in nanoparticles with average size of 31 ± 6 nm (*length*) and 8 ± 1 nm (*width*), i.e., aspect ratio (AR) around 3.9 (dimensions may vary from batch to batch), with LSPR band centred around 835 nm. To investigate the size change of nanorods, the Au reducing agent ratio (hidroquinone)/Au-seed was altered. By decreasing this molar ratio, it was possible to synthesize slightly longer rods 44 ± 8 nm (*length*) and 10 ± 1 nm (*width*), i.e., AR=4.4, with the LSPR band red-shifted to around 900 nm.

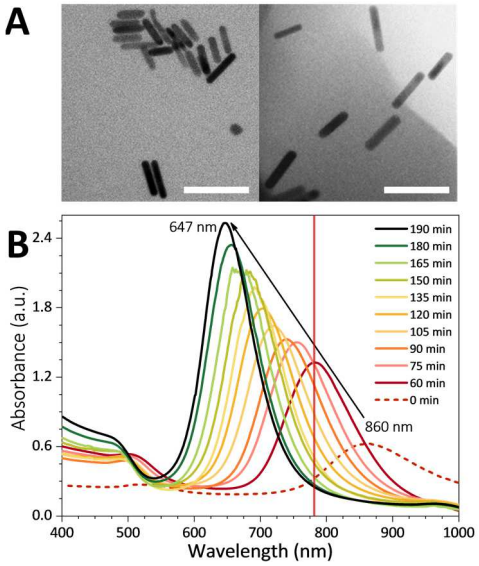

Figure III-1. (A) TEM images of Au nanorods with different aspect ratios (scale 100 nm). (B) Evolution of extinction spectra of colloidal solution of Au@Ag nanorods over Ag reduction time (vertical line represents the 785 nm laser line of conventional portable instruments).

The silver shell growth controlled over time can be monitored by the LSPR evolution (see Figure III-1B). Depending on the AR of the Au nanorods, the reaction time can be finely tuned to blue-shift the LSPR band to the region of interest. For example, after 180 min, pristine Au nanorods with AR=5.1 (47 ± 6 nm (*length*) and 9 ± 1 nm (*width*) yield Au@Ag nanorods with average size of 56 ± 12 nm (*length*) and 20 ± 2 nm (*width*), i.e., AR= 2.8. In the continuation, this work will present results for this system.

In the final Au@Ag@mSiO$_2$ nanostructures, the thickness of the mesoporous silica shell obtained with Au/TEOS molar ratio of 9.3 was 45 ± 8 nm. For template extraction, degradation of CTAB occurs above 150 ºC. The template removal efficiency accounts for 82% and 90% for reflux and ultrasonication methods respectively. The resulting silica efficiency for concentrating molecules on its mesopores was validated on our previous work [14]. Accordingly, the Au@Ag@mSiO$_2$ solution subjected to the "ultrasonication" method was selected for the spinning process on glass substrates.

The deposition of the Au@Ag@mSiO$_2$ on transparent substrates can be seen in Figure III-2, which shows the comparison between nanoparticles in colloidal (A) and in film assembly (B). The spin coated films circa 1 µm thick show considerable homogeneous surface at the microscale. The LSPR peaks of the resulting systhem (colloidal and film) are observed in Figure III-2 C. In this work, the similarities between the experimental LSPR bands observed for the ethanolic colloidal suspensions of both Au@Ag and Au@Ag@mSiO$_2$ nanorods (650-670 nm), are due the analogous dielectric constants of ethanol and mSiO$_2$, respectively.

When the Au@Ag@mSiO$_2$ nanoparticles are transferred to the glass substrate, the effective dielectric constant is reduced due the air surrounding the nanoparticles. The mesoporous surroundings of the Au@Ag nanorods can be described as an effective medium that depends on the mSiO$_2$ thickness. For thicknesses larger than the penetration length of the plasmon into the medium, the effective dielectric constant is that of the mSiO$_2$. On the contrary, for thinner mSiO$_2$ shells, the plasmon "sees" a different effective refractive index depending on the embedding medium, which likely explain the experimental blue-shifts of the LSPR from 670 nm to approximately 620 nm. Thus, the dielectric environment is critical in engineering the spectral location of these plasmonic resonances for SERS based gas sensing

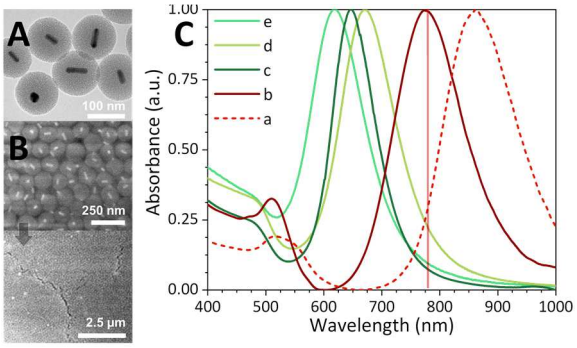

Figure III-2. (A) TEM image of Au@Ag@mSiO$_2$. (B) SEM images of Au@Ag@mSiO$_2$ films on glass. (C) LSPR bands of (a) Au nanorods, (b) Au@Ag nanorods at 80 min, (c) Au@Ag nanorods at 190 min, (d) Au@Ag@mSiO$_2$ colloidal and (e) Au@Ag@mSiO$_2$ film.

Following with the SERS efficiency, the calculated AEF value is 7.3x10^4 with a relative standard deviation (RSD) between the 3 data mappings of 10%. Results are presented at Figure III-3A, at the region of interest, i.e., around 1330 cm^{-1}. Reproducibility between substrates still need to be improved, showing an RSD of 52% between two replicas. Due to isolation of Au@Ag nanorods by the mSiO$_2$ shell, the plasmonic intercoupling between single nanoparticles is negligible, which explains the the relatively low AEF in comparison with other reported core-shell systems (Ag@MOF), with values of 6.4x10^6 [18]. For similar core-shell systhems, reported AEF had values of 1.2x10^3 [19].

It would be expected a SERS signal improvement when using 633 as Raman laser line. However, these experiments are out the scope due to 785 nm is the standard laser line of portable Raman instruments. On the contrary, SERS substrates prepared from Au nanorods with AR=4.4 (data not shown), would be clearly outperforming due to proximity of its plasmonic resonance to the laser line.

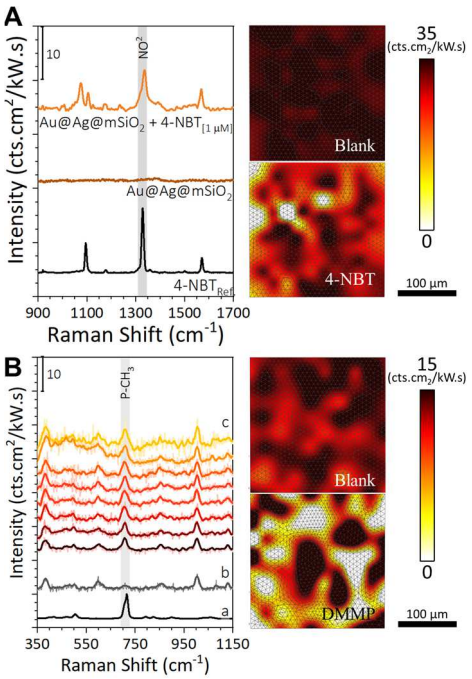

Figure III-3. SERS spectra of (A) 4-NBT and (B) DMMP on Au@Ag@mSiO$_2$ films on glass: (a) Raman reference spectrum, (b) blank of substrate, (c) spectra of targeted molecule on films.

The averaged SERS spectra of DMMP (2.5 ppmV) in gas phase are depicted in Figure III-3B. The characteristic Raman band of DMMP at 710 cm^{-1} is clearly observed in all the acquired SERS spectra. The gas detection capabilities of the SERS substrate is corroborated measuring the SERS intensity mappings in different locations. The uniformity of the SERS signal, assessed by the intensity color map of the reference DMMP band at 710 cm^{-1} (see Figure III-3B), is further improved by increasing the number of spin-coating cycles.

IV. Conclusions

Our core-shell Au@Ag@mSiO$_2$ nanoarchitecture is designed to have a spherical mesoporous silica shell to provide the surface area for adsorption and concentration of gaseous molecules, and an Au@Ag core whose LSPR band is finely tuning for the proper alignment with the laser line of the Raman instrument. According to our preliminary experiments with DMMP at 2.5 ppmV, the SERS substrates prepared from assembly of Au@Ag@mSiO$_2$ nanoparticles on transparent substrates arise as promising candidates for Raman SERS detection in gas phase of highly toxic and/or hazardous compounds. Future applications of this SERS substrate with portable Raman equipments are envisioned for in-field DIM in order to aid first responders during potential chemical treats, as proposed in the SERSing project.

Acknowledgment

This project has received funding from the European Union's Horizon 2020 research and innovation programme under grant agreements No 883390 (SERSing Project - sersing.eu) and No 823895 (SENSOFT Project).

V. REFERENCES

[1] F. Bruno *et al.*, "CBRN risk scenarios," *NATO Science for Peace and Security Series A: Chemistry and Biology*, pp. 309–317, 2018, doi: 10.1007/978-94-024-1304-5_23.

[2] B. J. Lukey, J. A. Romano, and Jr. H. Salem, *Biomedical and Psychological Effects, Medical Countermeasures, and Emergency Response*, vol. 3. 2019.

[3] A. Alcaraz, "Gas Chromatography/Mass Spectrometry in Analysis of Chemicals Relevant to the Chemical Weapons Convention," in *Encyclopedia of Analytical Chemistry*, John Wiley & Sons, Ltd, 2012. doi: 10.1002/9780470027318.a0405.pub2.

[4] M. A. Mäkinen, O. A. Anttalainen, and M. E. T. Sillanpää, "Ion mobility spectrometry and its applications in detection of chemical warfare agents," *Analytical Chemistry*, vol. 82, no. 23, pp. 9594–9600, Dec. 2010, doi: 10.1021/ac100931n.

[5] H. M. Brown, T. J. McDaniel, K. R. Doppalapudi, C. C. Mulligan, and P. W. Fedick, "Rapid,: In situ detection of chemical warfare agent simulants and hydrolysis products in bulk soils by low-cost 3D-printed cone spray ionization mass spectrometry," *Analyst*, vol. 146, no. 10, pp. 3127–3136, May 2021, doi: 10.1039/d1an00255d.

[6] M. Lafuente *et al.*, "Highly sensitive SERS quantification of organophosphorous chemical warfare agents: A major step towards the real time sensing in the gas phase," *Sensors and Actuators, B: Chemical*, vol. 267, pp. 457–466, 2018, doi: 10.1016/j.snb.2018.04.058.

[7] T. Kondo *et al.*, "Analysis of chemical warfare agents by portable Raman spectrometer with both 785 nm and 1064 nm excitation," *Forensic Science International*, vol. 291, pp. 23–38, Oct. 2018, doi: 10.1016/j.forsciint.2018.07.032.

[8] M. Lafuente, E. J. W. Berenschot, R. M. Tiggelaar, R. Mallada, N. R. Tas, and M. P. Pina, "3D fractals as SERS active platforms: Preparation and evaluation for gas phase detection of G-nerve agents," *Micromachines (Basel)*, vol. 9, no. 2, 2018, doi: 10.3390/mi9020060.

[9] M. Lafuente, D. Sanz, M. Urbiztondo, J. Santamaría, M. P. Pina, and R. Mallada, "Gas phase detection of chemical warfare agents CWAs with portable Raman," *Journal of Hazardous Materials*, vol. 384, no. September 2019, p. 121279, 2020, doi: 10.1016/j.jhazmat.2019.121279.

[10] D. Zhang, H. You, L. Zhang, and J. Fang, "Facile Surface Modification of Mesoporous Au Nanoparticles for Highly Sensitive SERS Detection," *Analytical Chemistry*, vol. 92, no. 23, pp. 15379–15387, Dec. 2020, doi: 10.1021/acs.analchem.0c02781.

[11] P. Y. Steinberg, M. M. Zalduendo, G. Giménez, G. J. A. A. Soler-Illia, and P. C. Angelomé, "TiO2 mesoporous thin film architecture as a tool to control Au nanoparticles growth and sensing capabilities," *Physical Chemistry Chemical Physics*, vol. 21, no. 20, pp. 10347–10356, 2019, doi: 10.1039/c9cp01896d.

[12] M. N. Sanz-Ortiz, K. Sentosun, S. Bals, and L. M. Liz-Marzán, "Templated Growth of Surface Enhanced Raman Scattering-Active Branched Gold Nanoparticles within Radial Mesoporous Silica Shells," *ACS Nano*, vol. 9, no. 10, pp. 10489–10497, 2015, doi: 10.1021/acsnano.5b04744.

[13] N. Zhou, X. Wang, and Z. Hu, "Control of structure of au@tio2 coreshell hollow microspheres with multiple nanocores and porous shells," *Chemistry Letters*, vol. 42, no. 9, pp. 1079–1081, 2013, doi: 10.1246/cl.130450.

[14] M. Lafuente *et al.*, "SERS Detection of Neurotoxic Agents in Gas Phase Using Microfluidic Chips Containing Gold-Mesoporous Silica as Plasmonic-Sorbent," in *2019 20th International Conference on Solid-State Sensors, Actuators and Microsystems and Eurosensors XXXIII, TRANSDUCERS 2019 and EUROSENSORS XXXIII*, Jun. 2019, pp. 1313–1316. doi: 10.1109/TRANSDUCERS.2019.8808289.

[15] V. Hornebecq, M. Antonietti, T. Cardinal, and M. Treguer-Delapierre, "Stable silver nanoparticles immobilized in mesoporous silica," *Chemistry of Materials*, vol. 15, no. 10, pp. 1993–1999, May 2003, doi: 10.1021/CM021353V/ASSET/IMAGES/MEDIUM/CM021353VN00001.GIF.

[16] E. Gergely-Fülöp, D. Zámbó, and A. Deák, "Thermal stability of mesoporous silica-coated gold nanorods with different aspect ratios," *Materials Chemistry and Physics*, vol. 148, no. 3, pp. 909–913, 2014, doi: 10.1016/J.MATCHEMPHYS.2014.08.069.

[17] L. Vigderman and E. R. Zubarev, "High-yield synthesis of gold nanorods with longitudinal SPR peak greater than 1200 nm using hydroquinone as a reducing agent," *Chemistry of Materials*, vol. 25, no. 8, pp. 1450–1457, Apr. 2013, doi: 10.1021/cm303661d.

[18] G. C. Phan-Quang *et al.*, "Tracking airborne molecules from afar: Three-dimensional metal-organic framework-surface-enhanced raman scattering platform for stand-off and real-time atmospheric monitoring," *ACS Nano*, vol. 13, no. 10, pp. 12090–12099, Oct. 2019, doi: 10.1021/acsnano.9b06486.

[19] P. A. Mercadal, L. A. Perez, and E. A. Coronado, "Optical Properties of Silica-Coated Au Nanorods: Correlating Theory and Experiments for Determining the Shell Porosity," *Journal of Physical Chemistry C*, vol. 125, no. 28, pp. 15516–15526, 2021, doi: 10.1021/acs.jpcc.1c02647.